Journal of Sound and Vibration (2000) **234**(4), 661–679
doi:10.1006/jsvi.2000.2867, available online at http://www.idealibrary.com on IDEAL®

STUDY ON DIFFERENT BEAM MODELS IN MOVING FORCE IDENTIFICATION

S. S. Law and X. Q. Zhu

Civil and Structural Engineering Department, The Hong Kong Polytechnic University, Hunghom, Kowloon, Hong Kong

(*Received* 25 *October* 1999; *and in final form* 17 *January* 2000)

Several methods have been developed recently to identify moving forces on a beam. The results from all of them exhibit fluctuations at the beginning and end of the time history and they are natural outcomes of the ill-conditioned inverse problem. Accuracy of the identified forces also depends on the parameters of the beam–force system which have not been systematically studied. This paper employs Tikhonov regularization technique to provide bounds to the ill-conditioned results in the identification problem. The calculation of the optimal regularization parameter is discussed. The improved algorithm is then used to study the effect of different parameters on the identification results through single-force and multi-forces identification. Both the Timoshenko beam theory and the Euler–Bernoulli beam theory are included in the study for a comparison. Laboratory results on two moving forces identification are also presented for illustration. Timoshenko beam model is found better than the Euler–Bernoulli beam model in the identification, and the limits of applications of the moving force identification method are also reported.

1. INTRODUCTION

The vehicle/bridge interaction forces are important to bridge design as they contribute to the live load component in the bridge design code. Direct measurement of the forces using instrumented vehicles are expensive and are subjected to bias [1, 2] while results from computation simulations are subjected to modelling errors [3–5]. Inclusion of the influencing parameters in the model for simulation would make it computationally expensive. Systems have been developed for weigh-in-motion of the vehicles [6, 7] but they all measure only the static axle loads. A technique to determine the vehicular loads from the vibration responses of the bridge deck is required such that the different parameters of the bridge and vehicle system are accounted for in the measured responses, and the cost involved would be much less than that by direct measurement.

There are generally four approaches to determine the forces from the structural dynamic responses. The time domain approach [8] models the structure and forces with a set of second order differential equations. The forces are represented as step functions in a small time interval. These equations of motion are then expressed in the model co-ordinates, and these uncoupled equations are solved by deconvolution in the time domain. The forces are then identified using the modal superposition principle. Zhu and Law [9] also identify a group of moving forces in the time domain. The bridge deck is modelled as a multi-span continuous Timoshenko beam with non-uniform cross-section, and the forces are modelled

0022-460X/00/290661 + 19 $35.00/0

as a group of moving loads. They are identified using the modal superposition and optimization technique. The frequency and time domains approach [10] performs Fourier transformation on the equations of motion, which are expressed in modal co-ordinates. The Fourier transforms of the responses and the forces are related in the frequency domain, and the time histories of the forces are found directly by the least-squares method. The modal approach [11] identifies the forces completely in the modal co-ordinates. Measured displacements are converted into modal displacements with an assumed shape function. The modal velocities and accelerations are then obtained by numerical means. The forces are then identified by solving the uncoupled equations of motion in modal co-ordinates. Law and Fang [12] also reported a state estimation approach in which the state-space formulation of the dynamic system is solved using dynamic programming with minimization of the errors between the measured and the reconstructed responses from the identified moving forces.

All the above works are based on an Euler–Bernoulli beam model which is not representative of most bridge decks with deep cross-sections. This paper studies the moving force identification with a Timishenko beam model and compares the result with that from an Euler–Bernoulli beam model. The solution for the forces is obtained using the Tikhonov [13] regularization method. Two methods to determine the optimal regularization parameter of the solution are discussed. Some factors which may pose limits to the application of the method are studied, which are namely, the number of sensors, vibration modal truncation, sampling frequency, spacing of forces, excitation frequency, and the measurement noise level. Computation simulations and laboratory tests results are presented to illustrate the comparison, and the limits of application of the method are reported.

2. MULTI-SPAN BEAM UNDER MOVING LOADS

Lee [14] and Zheng et al. [15] have studied the vibration behaviour of a multi-span continuous bridge modelled as a multi-span non-uniform continuous Euler–Bernoulli beam under a set of moving loads using different assumed mode shapes. Henchi and Fafard [16] used the same Euler–Bernoulli beam and finite element transfer matrix approach in a similar study. Wang and Lin [17] have studied the vibration of a T-frame bridge deck using Timoshenko beam model. In the present work, the vibration behaviour of a multi-span non-uniform Timoshenko beam subjected to a set of moving loads is analyzed basing on Hamilton principle with the intermediate point constraints represented by very stiff linear springs. The loads can take up any initial position on the beam.

Figure 1 shows a continuous beam with $(Q-1)$ intermediate point supports under N_f moving loads. The beam is constrained at these supports. The loads P_1 $(l = 1, 2, \ldots, N_f)$ are moving as a group at a prescribed velocity $v(t)$ along the axial direction of the beam from left to right. The load locations at time t are described as $\hat{x}_l(t)$ $(l = 1, 2, \ldots, N_f)$.

Expressing the transverse displacement $y(x, t)$ and angular rotation $\psi(x, t)$ of a beam cross-section in modal co-ordinates

$$\begin{aligned} y(x,t) &= \sum_{i=I}^{n} q_i(t) Y_i(x), \\ \psi(x,t) &= \sum_{i=I}^{n} q_i(t) \phi_i(x) \quad \{i = 1, 2, \ldots, n\}, \end{aligned} \tag{1}$$

where $\{Y_i(x), \phi_i(x),\ i = 1, 2, \ldots, n\}$ are the assumed vibration modes that satisfy the boundary conditions and $\{q_i(t),\ i = 1, 2, \ldots, n\}$ are the generalized co-ordinates. The

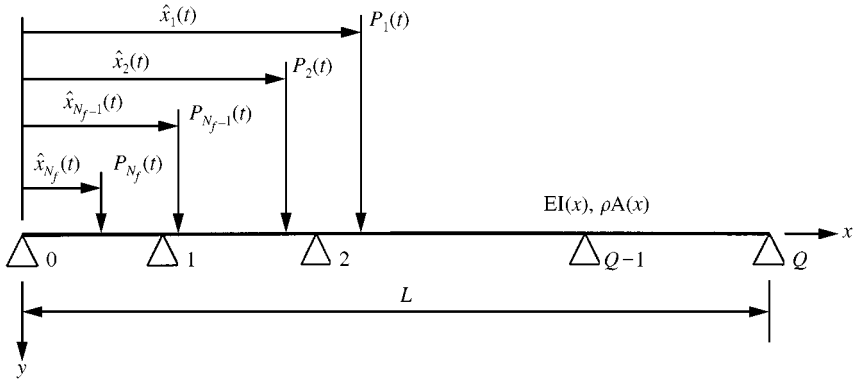

Figure 1. A continuous beam with intermediate point supports under a system of moving forces.

equations of motion can be written as shown in equation (2) based on the Hamilton principle [9]. This equation of motion should be representative of most highway bridges where the effect of deep cross-section has been accounted for:

$$M\ddot{q}(t) + C\dot{q}(t) + Kq(t) = F(t), \tag{2}$$

where

$$\begin{aligned} M &= \{m_{ij}, i = 1, 2, \ldots, n;\ j = 1, 2, \ldots, n\}, \\ K &= \{k_{ij}, i = 1, 2, \ldots, n;\ j = 1, 2, \ldots, n\}, \\ C &= \{C_{ij}, i = 1, 2, \ldots, n;\ j = 1, 2, \ldots, n\}, \\ q(t) &= \{q_1(t), q_2(t), \ldots, q_n(t)\}^{\mathrm{T}}, \\ F(t) &= \{f_1(t), f_2(t), \ldots, f_n(t)\}^{\mathrm{T}} \end{aligned} \tag{3}$$

and

$$\begin{aligned} m_{ij} &= \int_0^L \rho A(x)[Y_i(x)\,Y_j(x) + \gamma^2(x)\phi_i(x)\phi_j(x)]\,\mathrm{d}x, \\ k'_{ij} &= \int_0^L [EI(x)\phi'_i(x)\phi'_j(x) + \kappa GA(x)(Y'_i(x) - \phi_i(x))(Y'_j(x) - \phi_j(x))]\,\mathrm{d}x, \\ k''_{ij} &= k \sum_{l=1}^{Q-1} Y_i(x_l)\,Y_j(x_l), \\ k_{ij} &= k'_{ij} + k''_{ij}, \\ f_i(t) &= \sum_{l=1}^{N_f} P_l(t)\,Y_i(\hat{x}_l(t)) \quad (i = 1, 2, \ldots, n;\ j = 1, 2, \ldots, n), \end{aligned} \tag{4}$$

where G is the shear modulus of the beam material and $A(x)$ is the cross-sectional area, ρ is the density of material of the beam, E is the Young's modulus, $I(x)$ is the moment of inertia of the beam cross-section, $\gamma(x)$ is the radius of gyration of the beam cross-section, k is

the stiffness of the point constraints, κ is the shear coefficient, $x_i (i = 0, 1, 2, \ldots, Q)$ are coordinates of the intermediate point supports and end supports, $\dot{q}_i(t)$ and $\phi_i'(x)$ denote the first derivatives of $q_i(t)$ and $\phi_i(x)$, m_{ij} is the generalized mass, $f_i(t)$ is the generalized force, and k_{ij} is the generalized stiffness.

In Euler–Bernoulli beam theory, equation (4) can be written in a similar way as [14, 15]

$$
\begin{aligned}
m_{ij} &= \int_0^L \rho A(x)\, Y_i(x)\, Y_j(x)\, \mathrm{d}x, \\
k'_{ij} &= \int_0^L EI(x)\, Y_i''(x)\, Y_j''(x)\, \mathrm{d}x, \\
k''_{ij} &= k \sum_{l=1}^{Q-1} Y_i(x_l)\, Y_j(x_l), \\
k_{ij} &= k'_{ij} + k''_{ij}, \\
f_i(t) &= \sum_{l=1}^{N_f} P_l(t)\, Y_i(x_l(t)) \quad (i = 1, 2, \ldots, n;\ j = 1, 2, \ldots, n).
\end{aligned}
\tag{5}
$$

Since the assumed vibration modes have to satisfy the boundary conditions, the normal modes of a simply supported uniform beam proposed by Huang [18] are used in the present work

3. THEORY OF MOVING FORCE IDENTIFICATION

The transverse displacement $y(x_s, t)$ at measuring location x_s and at time t is expressed in modal co-ordinates,

$$
y(x_s, t) = \sum_{i=1}^{n} Y_i(x_s) q_i(t) \quad (s = 1, 2, \ldots, N_d), \tag{6}
$$

where N_d is the number of measuring points, and $Y_i(x_s)$ is the assumed mode at location x_s. Writing equation (6) in matrix form,

$$
\{y\}_{N_d \times 1} = [Y]_{N_d \times n} \{q\}_{n \times 1}, \tag{7}
$$

where $\{y\}_{N_d \times 1}$ is the lateral displacements at N_d measuring points. The least-squares solution of equation (6) is

$$
\{q\}_{n \times 1} = ([Y]^{\mathrm{T}}_{Nd \times n} [Y]_{Nd \times n})^{-1} [Y]^{\mathrm{T}}_{Nd \times n} [y]_{Nd \times 1}. \tag{8}
$$

The velocity and acceleration of the beam responses can then be obtained by numerical means from equations (7) and (8). If the central difference method is used to calculate the velocity and acceleration [19], it will induce a very large error. The following orthogonal polynomial [20] is adopted to model the displacement so as to avoid this error:

$$
y_k(t) = \sum_{i=1}^{N} a_i T_i(t) \tag{9}
$$

with

$$T_1 = \frac{1}{\sqrt{\pi}},$$

$$T_2 = \sqrt{\frac{2}{\pi}}\left(\frac{2}{T}t - 1\right),$$

$$T_3 = \sqrt{\frac{2}{\pi}}\left(2\left(\frac{2}{T}t - 1\right)^2 - 1\right), \tag{10}$$

$$T_{j+1} = 2\left(\frac{2}{T}t - 1\right)T_j - T_{j-1},$$

and $y_k(t)$ is the displacement at the kth measuring point. The velocity and acceleration are then approximated by the first and second derivatives of the orthogonal polynomial in equation (10) to have

$$\{y\}_{N_d\times 1} = [A]_{N_d\times N}[T]_{N\times 1}, \qquad \{\dot{y}\}_{N_d\times 1} = [A]_{N_d\times N}[\dot{T}]_{N\times 1}, \qquad \{\ddot{y}\}_{N_d\times 1} = [A]_{N_d\times N}[\ddot{T}]_{N\times 1}, \tag{11}$$

where $[A]_{N_d\times N}$, $[T]_{N\times 1}$, $[\dot{T}]_{N\times 1}$, $[\ddot{T}]_{N\times 1}$ are the coefficient matrix of the polynomial, the orthogonal polynomial variable matrix, the first and the second derivatives of the orthogonal polynomial variable matrix respectively. N is the order of the orthogonal polynomial The coefficient matrix of $[A]$ can then be obtained by the least-squares method from equation (11) as

$$[A]_{N_d\times N} = ([T]^{\mathrm{T}}_{N\times 1}[T]_{N\times 1})^{-1}[T]^{\mathrm{T}}_{N\times 1}\{y\}_{N_d\times 1}. \tag{12}$$

We substitute matrix $[A]$ back into equation (11) to get $\{\dot{y}\}$ and $\{\ddot{y}\}$. Again substituting $\{y\}$, $\{\dot{y}\}$ and $\{\ddot{y}\}$ into equation (8) and its derivatives, we get $\{q\}$, $\{\dot{q}\}$ and $\{\ddot{q}\}$, and equation (2) becomes

$$\{F\}_{n\times 1} = M_{n\times n}\{\ddot{q}\}_{n\times 1} + C_{n\times n}\{\dot{q}\}_{n\times 1} + K_{n\times n}\{q\}_{n\times 1}. \tag{13}$$

The generalized force vector $\{F\}$ can also be obtained from the last equation in equation (4) as

$$\{F\}_{n\times 1} = [B]_{n\times N_f}\{P\}_{N_f\times 1}, \tag{14}$$

where $\{P\}_{N_f\times 1}$ is the matrix of moving forces on the beam and

$$[B]_{n\times N_f} = \begin{bmatrix} Y_1(\hat{x}_1(t)) & Y_1(\hat{x}_2(t)) & \cdots & Y_1(\hat{x}_{N_f}(t)) \\ Y_2(\hat{x}_1(t)) & Y_2(\hat{x}_2(t)) & \cdots & Y_2(\hat{x}_{N_f}(t)) \\ \vdots & \vdots & \vdots & \vdots \\ Y_n(\hat{x}_1(t)) & Y_n(\hat{x}_2(t)) & \cdots & Y_n(\hat{x}_{N_f}(t)) \end{bmatrix}_{n\times N_f}. \tag{15}$$

The moving forces can then be calculated by least-squares method from equation (14) as

$$\{P\}_{N_f\times 1} = ([B]^{\mathrm{T}}_{n\times N_f}[B]_{n\times N_f})^{-1}[B]^{\mathrm{T}}_{n\times N_f})\{F\}_{n\times 1}. \tag{16}$$

But since the identified force $\{P\}$ is not a continuous function of the generalized forces $\{F\}$, solution to equation (15) is ill-conditioned with large fluctuations at the beginning and end of the time history [21]. A regularization method developed by Tikhonov [13] is used to provide bounds to the solution. The Tikhonov regularization method is based on the radical idea that minimizes the deviations of $[B]\{P\}$ from the unknown vector $\{F\}$ in equation (14) for a stable solution by means of an auxiliary non-negative parameter. This is equivalent to imposing certain constraints in the form of added penalty terms with adjustable weighting (regularization) parameters to the solution. One form of the Tikhonov function is written as follows:

$$J(\{P\}, \lambda) = \|[B]\{P\} - \{F\}\|^2 + \lambda\|\{P\}\|^2, \tag{17}$$

where λ is the non-negative regularization parameter. The solution of equation (16) can be obtained by minimizing the Tikhonov function in the damped least-squares method as [22]

$$\{P\}_{N_f\times 1} = ([B]^{\mathrm{T}}_{n\times N_f}[B]_{n\times N_f} + \lambda I)^{-1}[B]^{\mathrm{T}}_{n\times N_f}\{F\}_{n\times 1}, \tag{18}$$

where I is the identity matrix, and a singular-value decomposition is used in the pseudo-inverse calculation.

4. REGULARIZATION PARAMETER λ

The main difficulty of applying the Tikhnov regularization lies in the method to find the optimal regularization parameter λ. Two methods to find the optimal regularization parameter are presented in this paper. The use of either method depends on the availability of the true force. If the true forces are known, the true force $\{P\}^{(True)}$ is compared with the identified values $\{P\}^{(identify)}$, and an error curve, the S-curve [23] can be plotted for different values of λ as shown in Figure 2. The error of identification in the force time history is

$$error = \frac{\|\{P\}^{(identify)} - \{P\}^{(True)}\|}{\|\{P\}^{(True)}\|} \times 100\% \tag{19}$$

and $\|\cdot\|$ is the norm of a matrix. It is noted from Figure 2 that the optimal value of λ corresponds to the smallest error.

In the more practical case when $\{P\}^{(True)}$ is unknown as in experiment, the L-curve proposed by Hansen [24] is used to determine the optimal λ value. The L-curve is a plot of the seminorm of the solution against the residual norm. The norm of residuals E of the forces is calculated as

$$E = \|[B]\{P\}^{(identify)} - \{F\}\| \tag{20}$$

and for the first order regularization proposed by Busby and Trujillo [25], the seminorm of the estimated forces is

$$EI = \|\{P\}^{(identify)}_{j+1} - \{P\}^{(identify)}_{j}\|, \tag{21}$$

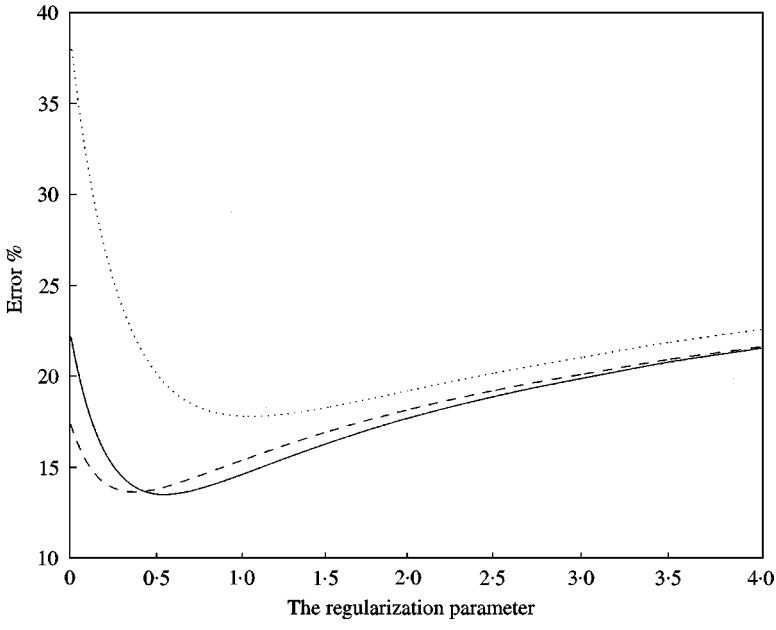

Figure 2. Typical S-curve (– – 1% noise; —5% noise; ... 10% noise).

where $\{P\}_j^{(identify)}$, $\{P\}_{j+1}^{(identify)}$ are the identified forces with λ_j and $\lambda_j + \Delta\lambda$. Typical L-curves are plotted in Figure 3 for different noise levels in the measured data, and they all exhibit a corner in each L-curve. The value of λ that corresponds to the point immediately to the right of the corner is the optimal value.

5. SIMULATION STUDIES

Both Timoshenko beam model and Euler–Bernoulli beam model are used in the simulation studies for a comparison of their usefulness in the force identification problem. The errors in the simulating results are calculated from equation (19). The moving forces are identified using the damped least-squares method [13] from equation (18), and the optimal regularization parameter λ is calculated by the L-curve method. The effects of different influencing parameters of the dynamic system on the identification results are studied in the following two examples. They are the number of sensors, vibration modal truncation, sampling frequency, spacing of forces, excitation frequency, and the measurement noise level. The road surface roughness is an important factor affecting the accuracy of the identification in the form of high-frequency noise in the result. This factor will be considered in a separate report including a vehicle model in the identification of vehicle axle loads.

Example 1 (Single moving force identification on a single-span beam). The following point load is moving on top of a single-span simply supported beam:

$$f(t) = 40000[1 + 0{\cdot}1\sin(10\pi t) + 0{\cdot}05\sin(40\pi t)]\ \mathrm{N}. \tag{22}$$

The parameters of the beam are as follows: $EI = 1{\cdot}274916 \times 10^{11}$ N m, $\rho = 7700\ \mathrm{kg\,m^{-3}}$, $\rho A = 12\,000$ kg/m, $L = 40$ m, $G = 77{\cdot}6 \times 10^9$ N m^2. The moving speed is constant at 40 m/s and the initial position of the force is at the left end of the beam. The shear coefficient κ is

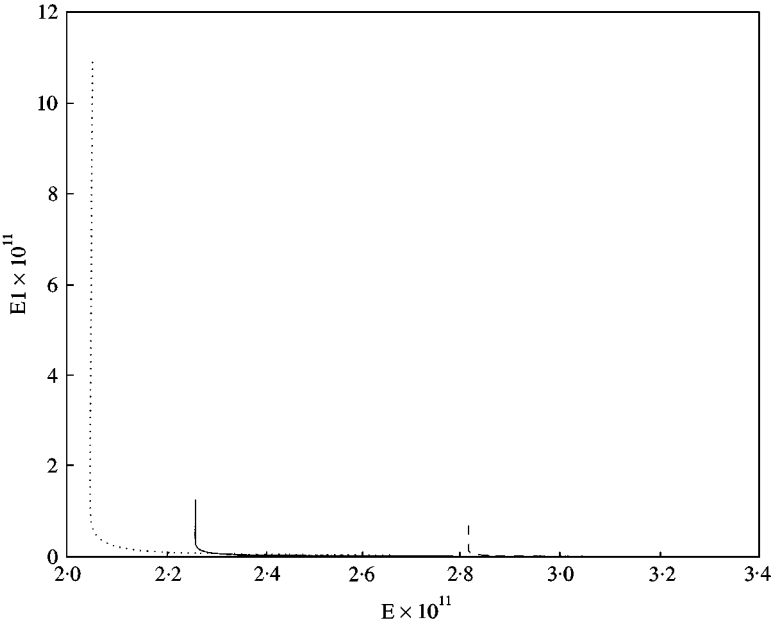

Figure 3. Typical L-curve (– – 1% noise; —5% noise; ... 10% noise).

$\frac{5}{6}$. The first three natural frequencies of the beam are 3·2, 12·8 and 28·8 Hz. The damping ratios for these three modes are all equal to 0·02. White noise is added to the calculated displacements to simulate the polluted measurement as

$$y = y_{calculated}(1 + Ep * N_{oise}),$$

where y is the measured response used for the identification, $y_{calculated}$ is the calculated response, E_P is the noise level and N_{oise} is a standard normal distribution vector (with zero mean value and unit standard deviation).

The first three modes are used in the calculation. Measured strains at 1/4L, 1/2L and 3/4L are used in the identification. The sampling frequency is 100 Hz. This example is used for Studies 1–5 describe below.

Study 1: *The optimal regularization parameter*: Table 1 shows the optimal value of λ and the corresponding errors for the two beam models. Since the true force is known, the optimal regularization parameter λ is determined from both the S-curve and L-curve methods, and they are the same for both beam models. The optimal value λ increases as the noise level increases, and yet the identified error and the norm are relatively stable. This result seems to indicate that the identified error is not sensitive to the noise level in the measurement. However, this result is based on a limited study, and the noise effect will be further studied below.

Study 2: *Effect of number of sensors*: The number of sensors is varied, and they are evenly distributed on the beam. Table 2 shows that the error in the identified forces has a significant reduction when the number of sensors is equal to or larger than the number of vibration modes used (which is three in this case) in the identification. This observation is consistent with the normal practice in vibration measurement of having one sensor for each vibration mode to be detected. The use of more sensors will not increase significantly the information collected for a particular set of modes to be monitored. Hence, the number of

TABLE 1

The optimal regularization parameter and error under different noise levels

Noise level (%)	Optimal λ	Error type	
		Error	Norm
1	0·37	13·65	$2{\cdot}83 \times 10^{11}$
5	0·54	13·50	$2{\cdot}29 \times 10^{11}$
10	1·05	17·80	$2{\cdot}16 \times 10^{11}$

TABLE 2

Error of identification with different numbers of sensors

Beam model	Noise level	Number of sensors					
		1	2	3	4	5	6
T	1%	105·6	23·4	13·7	13·7	13·7	13·7
	5%	103·5	22·9	13·5	13·5	13·5	13·5
	10%	103·5	26·0	17·8	17·8	17·8	17·8
E	1%	140·5	84·1	13·2	13·2	13·2	13·2
	5%	140·0	84·1	12·5	12·5	12·5	12·5
	10%	139·4	84·1	14·1	14·1	14·1	14·1

Note: T—Timoshenko beam; E—Euler–Benoulli beam.

sensors for the identification is recommended to be at least equal to the number of vibration modes in the study.

Study 3: *Effect of sampling frequency*: Table 3 shows the relation between the sampling frequency and the error in the identification with 5% noise level. The optimal λ is relatively stable indicating consistent quality in the identified results. The error remains relatively stable as the sampling frequency increases for both beam models. Therefore, the sampling frequency need not be very high in practice, and it may be taken as larger than two times the maximum frequency of interest to be consistent with the requirement in digital signal analysis. This recommendation means that the moving force identification method can use a relatively low sampling rate to be computationally efficient.

Study 4: *Effect of modal truncation*: Table 4 gives the errors in the identified force with different numbers of vibration modes when 5% noise level is included. The number of measuring points is taken equal to the number of vibration modes, and they are evenly located on the beam. The sampling frequency is two times the highest frequency of interest as suggested above. For a beam–force combination such as the one we have, the maximum natural frequency of the beam considered is larger than the highest frequency of interest or the exciting frequency of the moving force. The effect of higher modes is not included due to the low sampling rate used. As a result of this, the error in the identified force remains relatively the same and it does not depend on the number of vibration modes used. It is therefore recommended to determine the number of vibration modes from the highest frequency of interest.

TABLE 3

Error in identification with different sampling frequencies

Beam model		Sampling frequency (Hz)									
		100	200	300	400	500	600	700	800	900	1000
T	Error (%)	12·49	18·84	16·60	16·74	18·21	12·62	13·60	14·32	16·26	17·58
	λ	0·002	0·022	0·022	0·023	0·024	0·024	0·019	0·017	0·020	0·028
E	Error (%)	13·50	25·53	23·78	22·83	25·17	16·69	19·57	21·83	18·99	25·71
	λ	0·54	3·98	3·18	2·66	3·82	1·63	1·91	2·24	1·97	4·32

Note: T—Timoshenko beam; E—Euler–Benoulli beam.

TABLE 4

Error of identification with different numbers of vibration modes

Beam model		Number of modes									
		1	2	3	4	5	6	7	8	9	10
T	Error (%)	16·5	14·8	13·5	22·3	23·1	17·2	18·9	20·0	19·2	15·5
	λ	0·43	0·57	0·54	3·1	4·3	2·2	3·0	3·8	4·2	2·2
E	Error (%)	17·0	15·3	12·5	14·8	12·6	9·0	9·3	8·6	8·5	6·6
	λ	0·003	0·006	0·002	0·020	0·003	0·014	0·013	0·003	0·012	0·006

Note: T—Timoshenko beam; E—Euler–Benoulli beam.

Study 5: *Effect of exciting frequency*: The major exciting frequency of the force in equation (22) is varied from 0 to 50 Hz. Figure 4 shows the error of the identified force for each of the frequencies with 5% noise level. The error in the identified force increases when the exciting frequency of the moving force approaches the natural frequency of the beam–force system. The natural frequency of the beam–force system is smaller than that for the beam alone due to the existence of the force acting on top. The error around the third natural frequency identified by the Euler–Bernoulli beam model is larger than that by the Timoshenko beam model, but it is the opposite around the first natural frequency. The Timoshenko beam model in general gives larger error than the Euler–Bernoulli beam model over the whole range of frequencies studied.

Example 2 (Two moving forces identification on a two-span continuous beam). The following forces are crossing a two-span continuous beam:

$$f_1(t) = 20\,000[1 + 0{\cdot}1\sin(10\pi t) + 0{\cdot}05\sin(40\pi t)]\ \text{N},$$

$$f_2(t) = 20\,000[1 - 0{\cdot}1\sin(10\pi t) + 0{\cdot}05\sin(50\pi t)]\ \text{N}.$$

Note that there is an opposite component in the forces representing the pitching motion of a vehicle. The parameters of the beam are the same as in Example 1 except that the two beam span lengths are each 20 m. The stiffness of the intermediate support is 10^{16} N/m. The moving speed of the forces is again constant at 40 m/s and the initial position of the first force is at the left end of the beam. Five per cent noise is included in the measured responses.

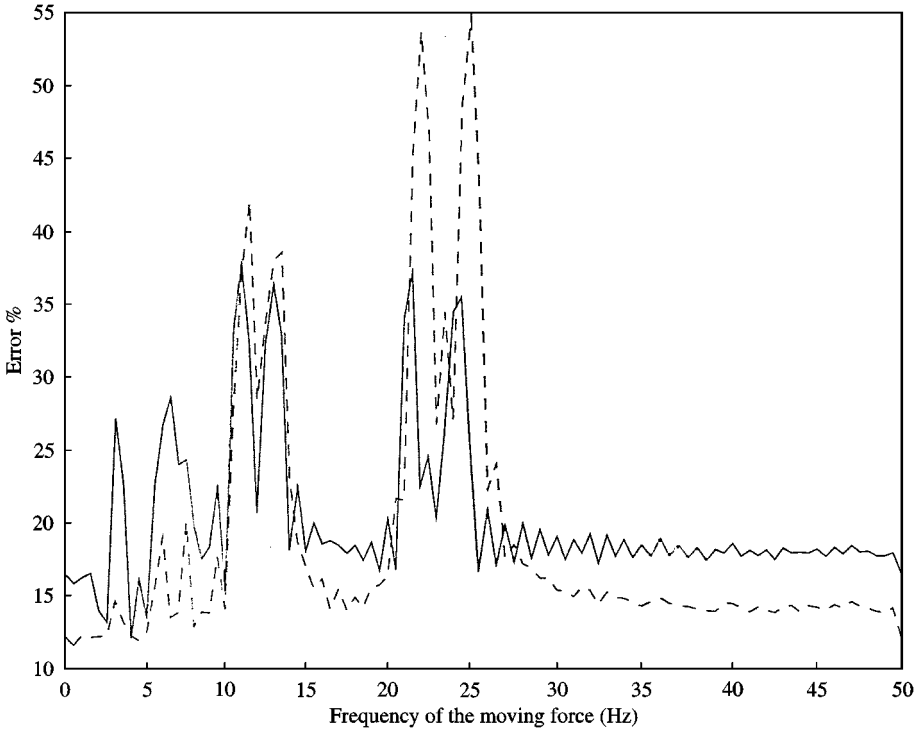

Figure 4. Error in identified force with different exciting frequencies: – – using Euler–Bernoulli beam model; — using Timoshenko beam model.

The first three modes are used in the identification. The measured displacements at 1/8L, 1/4L and 3/4L are used in the calculation. The sampling frequency is 200 Hz. This example is used for the Studies 6 and 7 described below.

Study 6: *Two moving forces identification*: Figures 5 and 6 show the identified forces using the Timoshenko beam theory and the Euler–Bernoulli beam theory. The curves are obtained after regularization, and they exhibit large discrepancies with the true forces at the beginning and end of the curves. Improvement to the results can be made by dividing the time history into smaller time segments. And different regularization parameters are used in each of these segments as done by Choi and Chang [25]. The identified results from the Timoshenko beam model and the Euler–Bernoulli beam model have no significant differences and they are close to each other throughout the time histories. It is also noted that the identified forces follow the main trend of the true forces except for some high-frequency components which are due to the 5% noise introduced in the analysis.

Study 7: *Effect of distance between two forces*: When two forces are close together, their effect on the dynamic response of a beam may not be easily differentiated, and the resolution of the two forces in the force identification may be reduced. Figure 7 shows the plot of errors of identification against the distance between the two moving forces at 5% noise level. The figure shows that the error increases monotonically as the distance between two moving forces increases with a smaller value at a shorter distance. This is contrary to the usual belief of having a larger error at a smaller spacing. Hence the moving force identification method can be used to identify two moving forces at a close spacing. The errors from the Timoshenko beam model and the Euler–Bernoulli beam model are similar with the former being slightly larger than the latter. Three peaks in the error curves are identified at 1·25, 2·5 and 3·75 Hz which are themselves harmonics. However their existence cannot be explained in this study.

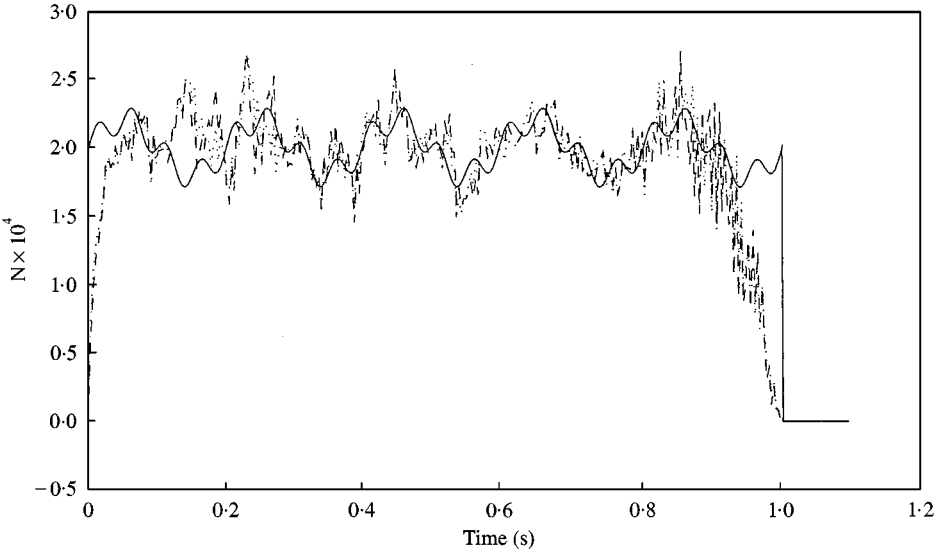

Figure 5. The identified first force with 5% noise: — true force; – – force from Timoshenko beam model; ... force from Euler–Bernoulli beam model.

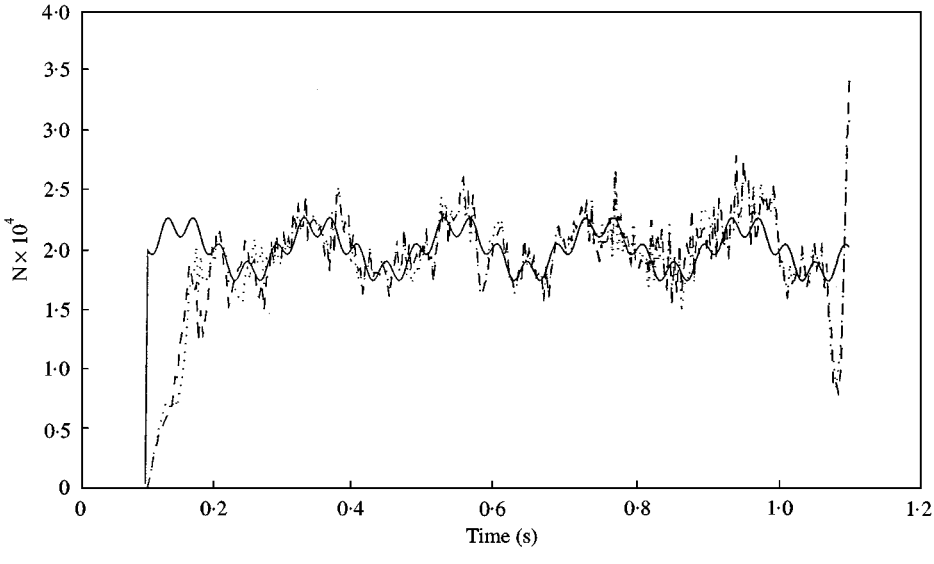

Figure 6. The identified second force with 5% noise: — true force; – – force from Timoshenko beam model; ... force from Euler–Bernoulli beam model.

6. LABORATORY EXPERIMENT WITH TWO MOVING FORCES

The experimental set-up is shown diagrammatically in Figure 8. The main beam, 3678 mm long with a 100 mm × 25 mm uniform cross-section, is simply supported. A U-shaped aluminum section is glued to the upper surface of the beams as a direction guide for the car. The model car is pulled along the guide by a string wound around the drive wheel of an electric motor. Seven photoelectric sensors are mounted on the beams to

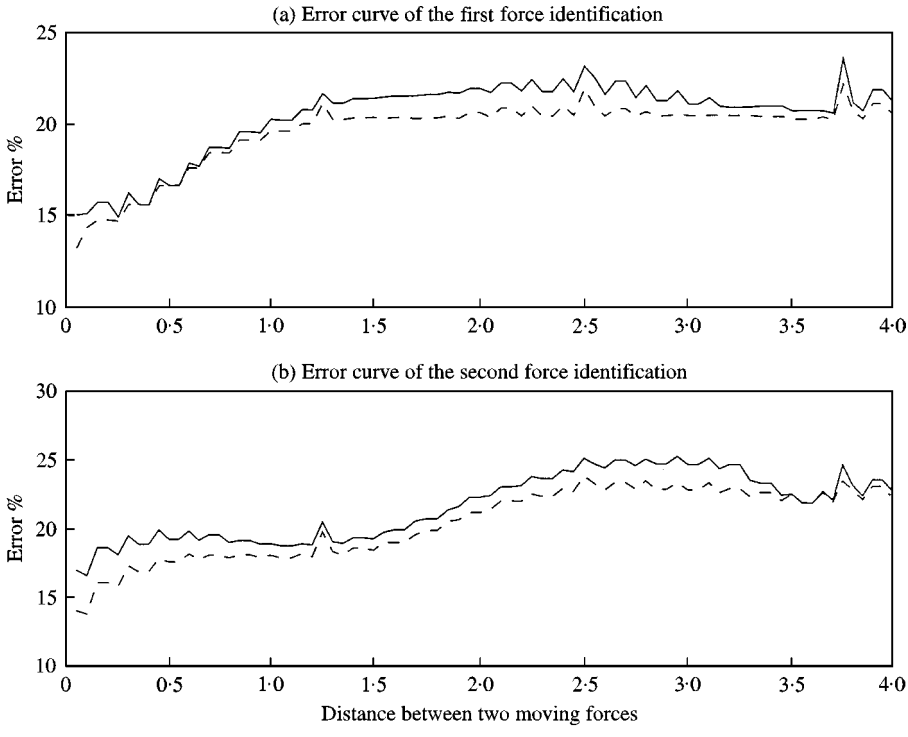

Figure 7. Effect if spacing of two forces on error in identification (with 5% noise). (a) Error curve of the first force identification. (b) Error curve for the second force identification: — from Timoshenko beam model; -- from Euler–Bernoulli beam model.

measure and monitor the moving speed of the car. They are located on the beam at roughly equal spacing of 0·776 m to check on the uniformity of the speed. Seven strain gauges are evenly located on the beam at one-eighth span spacing to measure the responses of the beam. A Data Translation DT2829 eight-channel dynamic A/D board is used for data collection in the experiment. The measured frequencies of the model car and the main beam are shown in Table 5. The sampling frequency is 2 kHz, and the data record time duration is 6 s. The model car has two axles at a space of 0·557 m and it runs on four rubber wheels. The mass of the whole car is 16·6 Kg.

The first three modes are used in the identification. Correlation coefficients are calculated between the measured strain and the strain reconstructed from the identified forces for 12 combinations of measured strains, and they are shown in Table 6. The Euler beam model gives slightly poorer correlation in all the cases than the Timoshenko beam model. There are two cases where the correlation is less than 0·3 while the latter model can still identify good results with a correlation above 0·7. However, the correlation coefficients vary with different combinations of measured information. Those derived from using more than three sensors are not much better than those from using three sensors. This confirms the result from Study 2.

The optimal regularization parameter λ is obtained from a modified plot of the L-curve by separately plotting the norm of the error and the seminorm of the solution against the parameter, and the intersection of the two curves gives the optimal value. The plot for the Timoshenko beam model and the Euler–Bernoulli beam model is shown in Figure 9, and both models give the same optimal value.

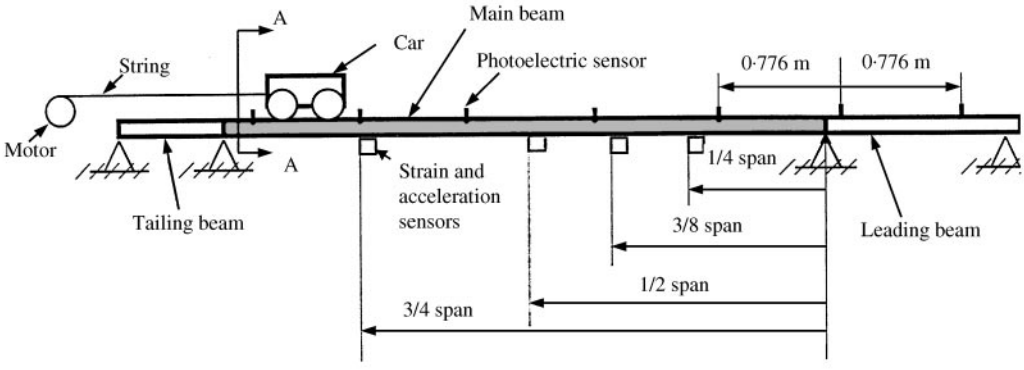

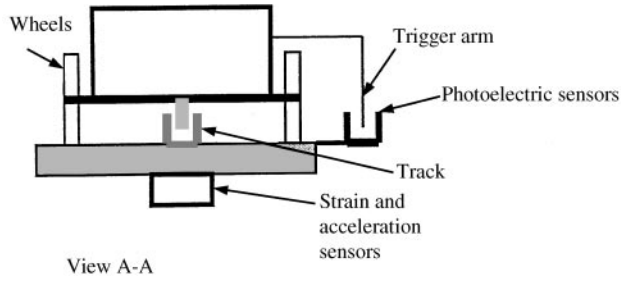

Figure 8. Diagrammatic drawing of experimental set-up.

TABLE 5

Natural frequencies of the model car and main beam

Mode	Model car (Hz)	Main beam (Hz)
1	7·82	3·67
2	9·77	16·83
3	11·72	37·83

Figures 10 and 11 show the identifying forces from strains at 1/4L, 1/2L and 3/4L. Only the results from the Timoshenko beam model with and without regularization are shown. Fluctuations in the time histories are found around 0·0 s, 0·5 s, 3·0 s and 3·6 s in the curves without regularization. These moments correspond to the entry of the first and second axles on the main beam and the exit of the first and second axles from the main beam, when the forcing system switches from single-force excitation to two-force excitation or *vice versa*. Such large fluctuations may also be caused by the gaps between the beam ends at the entry and exit which induce impulsive forces on the main beam. The fluctuations in the curves disappear after regularization, and the regularization has no effect on the time histories between these moments. These observations indicate that the regularization procedure only provides bounds to the ill-conditioned solutions without any smoothing effect. Errors in the curves in the form of high-frequency components has to be treated by some other means.

TABLE 6

Correlation coefficient between reconstructed and measured strains

Sensor combinations	Timoshenko beam model	Euler–Benoulli beam model
1/8s, 1/2s, 3/4s	0·939	0·900
1/4s, 1/2s, 3/4s	0·939	0·926
1/8s, 1/2s, 7/8s	0·943	0·897
1/8s, 1/4s, 1/2s	0·919	0·280
1/8s, 1/4s, 5/8s	0·901	0·564
1/8s, 1/4s, 7/8s	0·894	0·620
5/8s, 3/4s, 7/8s	0·729	0·278
1/8s, 1/4s, 3/4s, 5/8s	0·929	0·878
1/8s, 1/4s, 3/4s, 7/8s	0·893	0·657
1/8s, 1/4s, 1/2s, 3/4s, 7/8s	0·946	0·917
1/8s, 1/4s, 1/2s, 5/8s, 3/4s, 7/8s	0·941	0·909
1/8s, 1/4s, 5/8s, 7/8s	0·924	0·821

Note: 1/8s—mesured strain at 1/8 span.

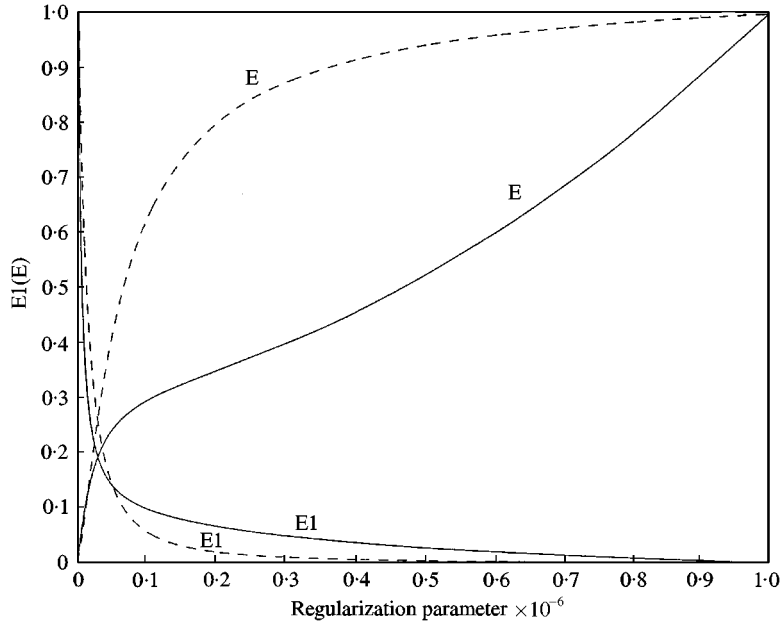

Figure 9. The modified L-curve; — Timoshenko beam model; -- Euler–Bernoulli beam model.

Figure 12 shows the reconstructed strains from the identified forces obtained from the Timoshenko beam model and the measured strain at $\frac{3}{8}$ span. The reconstructed strain varies around the curve of measured strain with some high-frequency components which are due to the measurement noise.

The two identified forces are added together and the resultant is shown in Figure 13. The curve is higher than the static curve in the first half of the time history and it is lower than the static curve in the second half. This arises from the deflection of the beam under its own weight. The model car accelerates downwards in the first half of the beam and it decelerates

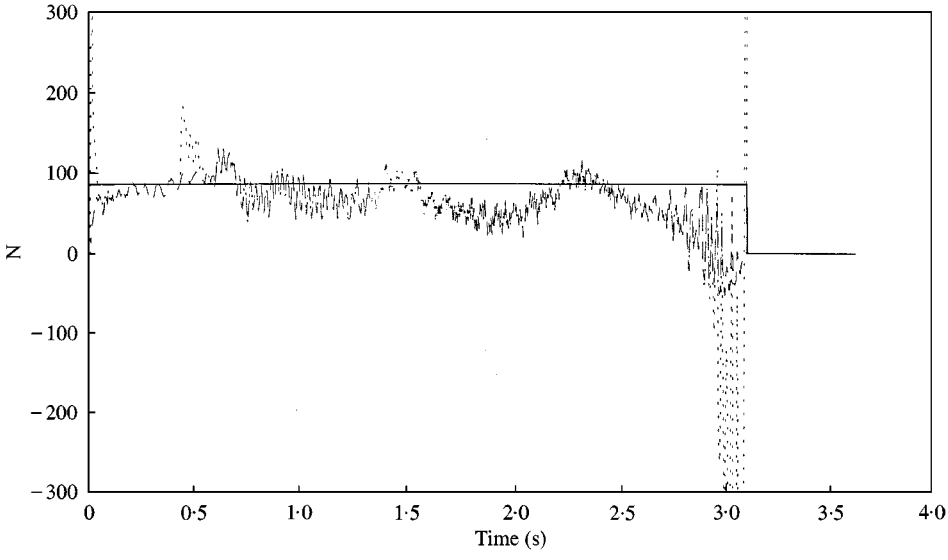

Figure 10. The first identified force from experiment using Timoshenko beam model: — static force; ..... without regularization; – – with regularization.

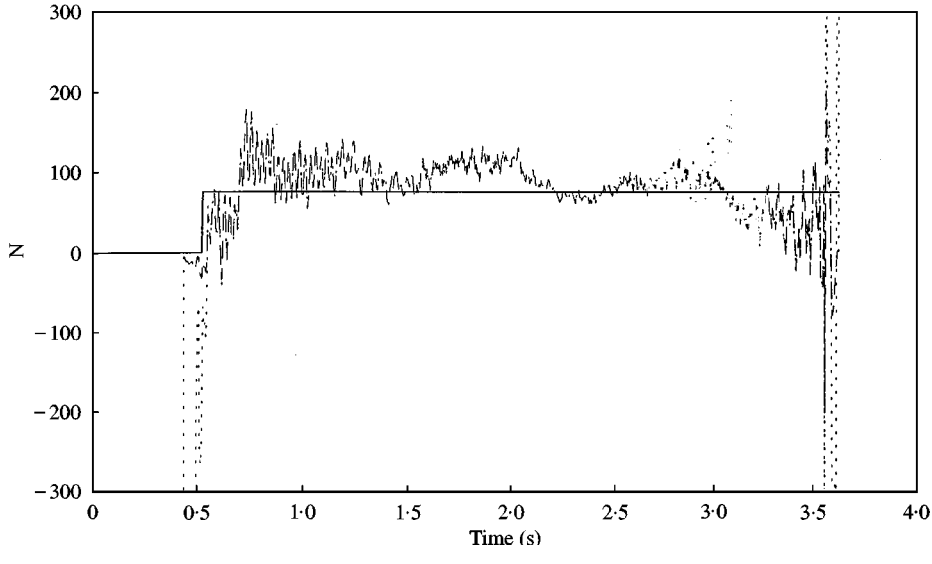

Figure 11. The second identified force from experiment using Timoshenko beam model: — static force; ..... without regularization; – – with regularization.

upwards in the second half of the beam. The differences from the static curve are due to these acceleration forces. The resultant force obtained from regularization is close to the static weight from the car, and is a good indication of the accuracy of the moving force identification method in identifying the resultant force of a system of moving forces.

7. CONCLUSIONS

A moving force identification method has been improved with a regularization procedure applied to the identified results. The ill-conditioned identified forces at the beginning and

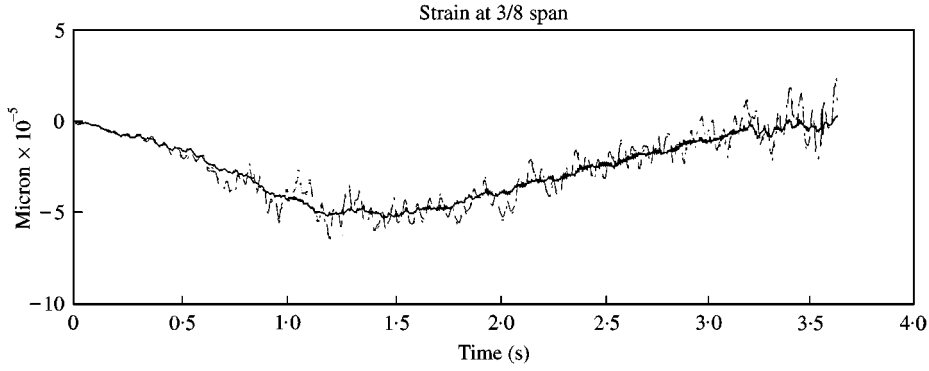

Figure 12. The measured and reconstructed strain at 3/8 span from experiment: — measured; ..... without regularization; – – with regularization.

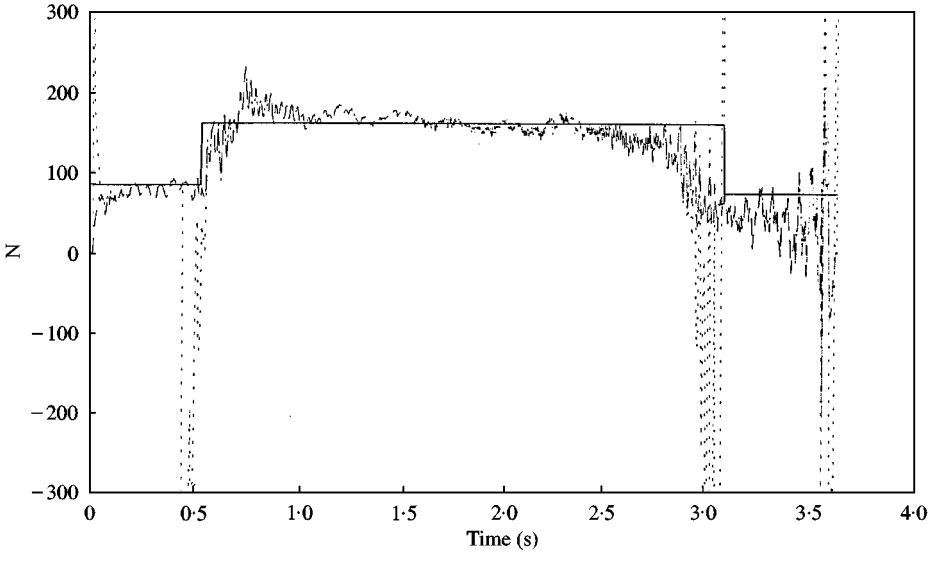

Figure 13. The identified resultant force from experiment: — static force; ..... without regularization; – – with regularization.

end of the time history are significantly improved. The regularization procedure does not have any smoothing effect on the results. The Timoshenko beam model gives better results in general than the Euler–Bernoulli beam model.

Limits on the application of this force identification method are studied, and the following recommendations are reported: The number of modes required in the identification depends entirely on the highest frequency of interest. The sampling frequency may be taken as two times the highest frequency of interest which may be the maximum exciting frequency of the moving force or the natural frequency of the beam. The number of sensors is recommended to be at least equal to the number of vibration modes in the analysis. The error in the identified forces becomes large when the exciting frequency of the moving force comes close to the natural frequency of the beam–force system. The error of identification is not sensitive to the distance between the two moving forces. Therefore, two forces moving at a close spacing can be resolved by this method.

ACKNOWLEDGMENT

The work described in this paper was supported by a grant from the Hong Kong Polytechnic University Research Funding Project No. V653.

REFERENCES

1. R. CANTINENI 1992 *Swiss Federal Laboratories for Materials Testing and Research* (*EMPA*) *Report No*. 220, 240 p. Dynamic behaviour of highway bridges under the passage of heavy vehicles.
2. R. J. HEYWOOD 1994 *International Journal of Vehicle Design*. Influence of truck suspensions on the dynamic response of a short span bridge.
3. M. F. GREEN and D. CEBON 1994 *Journal of Sound and Vibration* **170**, 51–78. Dynamic response of highway bridges to heavy vehicle loads: Theory and experimental validation.
4. Y. B. YANG and J. D. YAU 1997 *Journal of Structural Engineering*, *ASCE* **123**, 1512–1518. Vehicle-bridge interaction element for dynamic analysis.
5. K. HENCHI, M. FAFARD, M. TALBOT and G. DHATT 1988 *Journal of Sound and Vibration* **212**, 663–683. An efficient algorithm for dynamic analysis of bridges under moving vehicles using a coupled modal and physical components approach.
6. R. J. PETERS 1984 *Proceedings of 12th ARRB Conference*, vol. **12**, 10–18. A System to obtain vehicle axle weights.
7. R. J. PETERS 1986 *Proceedings of 13th ARRB and 5th REAAA Combined Conference* Part 6, 70–83. An unmanned and undetectable highway speed vehicle weighing system.
8. S. S. LAW, T. H. T. CHAN and Q. H. ZENG 1997 *Journal of Sound and Vibration* **201**, 1–22. Moving force identification: a time domain method.
9. X. Q. ZHU and S. S. LAW 1999 *Journal of Sound and Vibration* **228**, 377–396. Moving forces identification on a multi-span continuous bridge.
10. S. S. LAW, T. H. T. CHAN and Q. H. ZENG 1999 *Journal of Dynamic Systems, Measurement and Control ASME* **12** 394–401. Moving force identification: a frequency and time domains analysis.
11. T. H. T. CHAN, S. S. LAW, T. H. YUNG and X. R. YUAN 1998 *Journal of Sound and Vibration* **219**, 503–524. An interpretive method for moving force identification.
12. LAW and FANG 1999.
13. A. N. TIKHONOV 1963 *Soviet Mathematics* **4**, 1035–1038. On the solution of ill-posed problems and the method of regularization.
14. H. P. LEE 1994 *Journal of Sound and Vibration* **171**, 361–368. Dynamic response of a beam with intermediate point constraints subject to a moving load.
15. D. Y. ZHENG, Y. K. CHEUNG, F. T. K. AU and Y. S. CHENG 1998 *Journal of Sound and Vibration* **212**, 455–467. Vibration of multi-span non-uniform beams under moving loads by using modified beam vibration functions.
16. K. HENCHI and M. FAFARD 1997 *Journal of Sound and Vibration* **199**, 33–50. Dynamic behaviour of multi-span beams under moving loads.
17. R. -T. WANG and J. -S. LIN 1998 *Structural Engineering and Mechanics* **6**, 229–243. Vibration of T-type Timoshenko frames subjected to moving loads.
18. T. C. HUANG 1961 *Journal of Applied Mechanics* **28**, 578–584. The effect of rotatory inertial and of shear deformation on the frequency and normal mode equations of uniform beams with simple and conditions.
19. C. O'CONNOR, T. H. T. CHAN 1988 *Journal of Structural Engineering*, ASCE **114**, 1703–1723. Dynamic wheel loads from bridge strains.
20. F. ZHANG and D. M. ZHU 1996 *Journal of Nanjing University of Aeronautics and Astronautics* **28**, 755–760. A new theoretical study of dynamic load identification based on generalized polynomial expansion.
21. V. A. MOROZOV 1984 *Methods for Solving Incorrectly Posed Problems*. Berlin: Springer-Verlag, 1–64.
22. J. C. SANTANTAMARINA and D. FRATTA 1998 *Introduction to Discrete Signals and Inverse Problems in Civil Engineering*, 200–238. New York: ASCE Press.
23. H. R. BUSBY and D. M. TRUJILLO 1997 *Computers and Structures* **63**, 243–248. Optimal regularization of an inverse dynamics problem.

24. P. C. HANSEN 1992 *SIAM Review* **34**, 561–580. Analysis of discrete ill-posed problems by means of the L-curve.
25. K. Y. CHOI and F. K. CHANG 1996 *AIAA Journal* **34**, 136–142. Identification of impact force and location using distributed sensors.

APPENDIX A: NOMENCLATURE

$A(x)$	area of cross-section
E	norm of residuals
EI	seminorm of estimated forces
$EI(x)$	flexural stiffness of beam
F	generalized force matrix
G	shear modulus
K	generalized stiffness matrix
L	span length of beam
M	bending moment
M	generalized mass matrix
$P_i(t)$	ith moving load
$\{P\}_i^{(est)}$	estimated force with λ_j
c_{ij}	generalized damping
$f_i(t)$	ith generalized force
k	stiffness of point constraint
k_{ij}	generalized stiffness
m_{ij}	generalized mass
$q_i(t)$	ith generalized co-ordinate
$v(t)$	speed of moving load
x_i	initial position of ith moving load
x_l	location of measurement location
$Y_i(x_s)$, $\phi_i(x)$	assumed displacement mode shapes
$y(x, t)$	displacement function of beam
$\delta(t)$	Dirac delta function
$\varepsilon(x_s, t)$	measured strain at location x_s
κ	shear coefficient
λ	regularization parameter
$\gamma(x)$	radius of gyration of cross-section
$\psi(x, t)$	angle of rotation of cross-section
$\|\cdot\|$	norm of a vector of matrix